



Signals for vector-like leptons in an S_3 -symmetric 2HDM at ILC

Indrani Chakraborty^{1,a}, Dilip Kumar Ghosh^{2,b}, Nivedita Ghosh^{3,c}, Santosh Kumar Rai^{3,d}

¹ Department of Physics, Indian Institute of Technology, Kanpur 208 016, India

² School of Physical Sciences, Indian Association for the Cultivation of Science, 2A & 2B, Raja S.C. Mullick Road, Kolkata 700032, India

³ Regional Centre for Accelerator-based Particle Physics, Harish-Chandra Research Institute, A CI of Homi Bhabha National Institute, Chhatnagar Road, Jhansi, Prayagraj 211019, India

Received: 17 February 2022 / Accepted: 31 May 2022 / Published online: 17 June 2022

© The Author(s) 2022

Abstract In this work, we explore the signals of an S_3 -symmetric two Higgs doublet model with two generations of vector-like leptons (VLLs) at the proposed International Linear Collider (ILC). The lightest neutral component of the VLL in this model provides a viable dark matter (DM) candidate satisfying the current relic density data as well as circumventing all direct and indirect DM search constraints. Some representative benchmark points have been selected with low, medium and high DM masses, satisfying all theoretical and experimental constraints of the model and constraints coming from the DM sector. The VLLs (both neutral and charged) will be produced in pair leading to multi-lepton and multi-jet final states. We show that the ILC will prove to be a much more efficient and useful machine to hunt for such signals compared to LHC. Using traditional cut-based analysis as well as sophisticated multivariate analysis, we perform a detailed analysis of some promising channels containing mono-lepton plus di-jet, di-lepton, four-lepton and four jets along with missing transverse energy in the final state at 1 TeV ILC.

1 Introduction

The particle spectrum of the Standard Model (SM) being complete with the Higgs boson discovery [1,2] still leaves unanswered questions on our understanding of Nature. In a more complete picture being established, the SM can be better termed as an effective theory sustainable up to a certain scale. To circumvent the theoretical and experimental shortcomings, several extensions of the SM have been proposed in the literature exploiting new symmetries or mod-

ifications to the space-time with additional spatial dimensions to name a few. In each such extension addition of either bosonic or fermionic fields somewhat becomes inevitable. A typical extension which addresses some of the issues in the flavor sector of particle phenomenology involves vector-like fermions with vector-like leptons (VLL) as a natural entity. Unlike the SM fermions, the left- and right-chiral components of VLLs transform identically under the SM gauge symmetry. Some beyond SM extensions where such exotic fermions appear naturally are grand unified theories [3–6], theories with non-minimal supersymmetric extensions [7–13], warped or universal extra-dimension [14–22], composite Higgs model [23–29] and little Higgs model [30–34]. The phenomenology of additional VLLs is expected to be similar to excited leptons or can differ if the model predicts additional particles in the spectrum. The VLLs can also modify the SM Higgs boson decay to di-photon mode. The VLLs are however less constrained than chiral fourth generation of SM fermions, typically from electroweak precision observables and Higgs signal strengths [35]. The VLLs have also been studied in the context of dark matter (DM) phenomenology and several DM and collider searches have been performed in the framework containing SM augmented with Higgs singlet [36], Higgs doublet [37–40], Higgs triplet [35,41,42], left right symmetric model [43–45] extended by one or more generations of VLLs.

In the present analysis, we study an S_3 -symmetric two Higgs doublet model (2HDM) [46,47], along with two generations of VLLs. The addition of two generations of VLLs in this model helps guarantee an S_3 -symmetric Yukawa Lagrangian providing an aesthetic picture to their inclusion. The main motivation of S_3 -symmetric 2HDM is to provide proper mass hierarchy and mixing among the SM fermions. Besides, the S_3 -symmetric 2HDM incorporates a 125 GeV SM-like Higgs boson in a very simple and natural way, unlike in a general 2HDM [46,47]. In our model we impose an addi-

^a e-mail: indranic@iitk.ac.in (corresponding author)

^b e-mail: tpdkg@iacs.res.in

^c e-mail: niveditaghosh@hri.res.in

^d e-mail: skrai@hri.res.in

tional Z_2 symmetry, under which all the SM fermions are even and the VLLs are odd [48]. Thus the mixing between the SM fermions and VLLs is forbidden throughout the analysis, and the lightest neutral VLL serves as a viable DM candidate which satisfies correct relic density, direct detection cross-sections and thermally averaged annihilation cross-sections in indirect detection obtained from the experiments [48]. A rigorous collider analysis of the multi-leptons + missing transverse energy final state at high-luminosity (HL) LHC can be found in one of our recent studies [48] where we found that the LHC provided us with a limited sensitivity for the VLLs for large masses as well as when the spectrum satisfying DM results demanded a compressed spectrum. Such spectrums will be more likely to be observable in a cleaner environment of an electron–positron collider such as the International Linear Collider (ILC) [49,50]. The ILC will be an invaluable machine with several exciting physics studies and is hence proposed to run at several center of mass energies, each driven by the physics study it aims to achieve. For our analysis, we have chosen the high energy option of $\sqrt{s} = 1$ TeV that allows a larger phase space to produce heavier VLLs. In this work, we therefore study leptonic and hadronic states with missing transverse energy at 1 TeV ILC to highlight the sensitivity. We observed that the benchmarks with high DM masses or with a compressed particle spectrum which were challenging to probe owing to small signal cross-sections at HL-LHC are easily discernible with high significance in specific final states involving hadronic final states. To perform our collider analysis we select some benchmark points with low, medium and high DM masses from the multi-dimensional parameter space satisfying the theoretical, experimental and DM constraints. There exist several searches by ATLAS and CMS involving di-lepton [51], four leptons [52,53] and multi jets [54] along with missing transverse energy in the final states. We have validated all the benchmark points with the limits arising out of these existing studies. To optimize the signal over the SM backgrounds, for each channel we have performed a cut-based analysis and also shown the possible improvement in the analysis employing machine learning with a sophisticated multivariate technique.

The paper is organized as follows. In Sect. 2, we discuss the relevant scalar and Yukawa sector of the model. In Sect. 3, we present a collider analysis of the leptonic and hadronic final states along with missing transverse energy. Finally we summarize and conclude in Sect. 4.

2 Model

We work in the S_3 -symmetric 2HDM which contains two generations of VLLs. Including two generations of VLLs instead of one allows one to write a Yukawa Lagrangian fully

Table 1 $SU(2)_L \times SU(3)_C \times U(1)_Y \times Z_2$ quantum numbers assigned to the particles in the model

Fields	$SU(2)_L$	$SU(3)_L$	$U(1)_Y$	Z_2
ϕ_1	2	1	+1	1
ϕ_2	2	1	+1	1
$Q_{iL}, i = 1, 2, 3$	2	3	$+\frac{1}{3}$	1
$u_{iR}, i = 1, 2, 3$	1	3	$+\frac{4}{3}$	1
$d_{iR}, i = 1, 2, 3$	1	3	$-\frac{2}{3}$	1
$L_{iL}, i = 1, 2, 3$	2	1	-1	1
$e_{iR}, i = 1, 2, 3$	1	1	-2	1
$L'_{Li}, i = 1, 2$	2	1	-1	-1
$L''_{Ri}, i = 1, 2$	2	1	-1	-1
$e'_{Ri}, i = 1, 2$	1	1	-2	-1
$e''_{Li}, i = 1, 2$	1	1	-2	-1
$\nu'_{Ri}, i = 1, 2$	1	1	0	-1
$\nu''_{Li}, i = 1, 2$	1	1	0	-1

S_3 -symmetric. Each generation of VLL comprises of one left-handed lepton doublet L'_{Li} , one right-handed charged lepton singlet e'_{Ri} and one right-handed singlet neutrino ν'_{Ri} , accompanied by their mirror counter parts with opposite chirality, i.e. L''_{Ri} , e''_{Li} and ν''_{Li} with $i = 1, 2$. The quantum numbers for the SM and beyond Standard Model (BSM) particles are shown in Table 1, while Table 2 shows the S_3 quantum numbers of the particles. Two Higgs doublets ϕ_1 and ϕ_2 together form an S_3 -doublet. In Table 1, Q_{iL} , L_{iL} are the SM left-handed quark and lepton doublets, while u_{iR} , d_{iR} , e_{iR} are the right-handed up-type, down-type quark and charged lepton singlets respectively for $i = 1, 2, 3$.

2.1 Scalar and Yukawa Lagrangian

Two $SU(2)_L$ doublets ϕ_1 and ϕ_2 in S_3 -symmetric 2HDM with hypercharge $Y = +1$, jointly behave like a doublet under S_3 -symmetry, i.e. $\Phi = \begin{pmatrix} \phi_1 \\ \phi_2 \end{pmatrix}$.

The neutral components of ϕ_i acquire vacuum expectation value (responsible for the spontaneous symmetry breaking (SSB) of SM gauge symmetry). The doublets can be written as shown below,

$$\phi_i = \begin{pmatrix} \phi_i^+ \\ \frac{1}{\sqrt{2}}(v_i + h_i + i\rho_i) \end{pmatrix} \quad (1)$$

Here v_i 's are VEVs of two doublets with $v_1 = v \cos \beta$, $v_2 = v \sin \beta$ and $v = \sqrt{v_1^2 + v_2^2} = 246$ GeV. The ratio of two vacuum expectation values can be denoted by $\tan \beta$, i.e. $\tan \beta = \frac{v_2}{v_1}$.

The most general renormalisable scalar potential for S_3 -symmetric 2HDM can be written as the sum of $V_2(\phi_1, \phi_2)$ and $V_4(\phi_1, \phi_2)$ [46]:

Table 2 S_3 quantum number assigned to the particles in the model

Particles	S_3
$\begin{pmatrix} \phi_1 \\ \phi_2 \end{pmatrix}; \begin{pmatrix} Q_{1L} \\ Q_{2L} \end{pmatrix}; \begin{pmatrix} u_{1R} \\ u_{2R} \end{pmatrix}; \begin{pmatrix} d_{1R} \\ d_{2R} \end{pmatrix}; \begin{pmatrix} \ell_{1L} \\ \ell_{2L} \end{pmatrix}; \begin{pmatrix} e_{1R} \\ e_{2R} \end{pmatrix}$	2
$Q_{3L}, u_{3R}, d_{3R}, \ell_{3L}, e_{3R}$	1
$\begin{pmatrix} L'_{L1} \\ L'_{L2} \end{pmatrix}; \begin{pmatrix} L''_{R1} \\ L''_{R2} \end{pmatrix}; \begin{pmatrix} e'_{R1} \\ e'_{R2} \end{pmatrix}; \begin{pmatrix} e''_{L1} \\ e''_{L2} \end{pmatrix}; \begin{pmatrix} \nu'_{R1} \\ \nu'_{R2} \end{pmatrix}; \begin{pmatrix} \nu''_{L1} \\ \nu''_{L2} \end{pmatrix}$	2

$$V(\phi_1, \phi_2) = V_2(\phi_1, \phi_2) + V_4(\phi_1, \phi_2) \tag{2}$$

with

$$V_2(\phi_1, \phi_2) = m_{11}^2(\phi_1^\dagger\phi_1) + m_{22}^2(\phi_2^\dagger\phi_2) - \{m_{12}^2(\phi_1^\dagger\phi_2) + \text{h.c.}\} \tag{3}$$

and

$$V_4(\phi_1, \phi_2) = \lambda_1(\phi_1^\dagger\phi_1 + \phi_2^\dagger\phi_2)^2 + \lambda_2(\phi_1^\dagger\phi_2 - \phi_2^\dagger\phi_1)^2 + \lambda_3\{(\phi_1^\dagger\phi_2 + \phi_2^\dagger\phi_1)^2 + (\phi_1^\dagger\phi_1 - \phi_2^\dagger\phi_2)^2\}. \tag{4}$$

In Eqs. (3) and (4), the subscripts denote the dimensionality of the terms. The hermiticity of the scalar potential in Eq. (4), forces the quartic couplings λ_1, λ_2 and λ_3 to be real. In $V_2(\phi_1, \phi_2)$, m_{11}^2, m_{22}^2 are real, m_{12}^2 can be complex in principle. In this analysis, we shall not consider m_{12}^2 to be complex to circumvent CP -violation. The configuration $m_{11}^2 = m_{22}^2$ along with $m_{12}^2 = 0$ makes the quadratic part of the potential S_3 -symmetric. At the same time this condition results in a massless heavy Higgs boson [46]. Thus to avoid any other massless heavy Higgs boson apart from the Goldstone bosons, we adhere to: $m_{11}^2 = m_{22}^2$ and $m_{12}^2 \neq 0$. Thus the value of $\tan \beta$ is fixed to 1, following the minimisation conditions of the scalar potential in Eq. (2) [46].

The particle spectrum of this model comprises of SM-like Higgs (h), heavy CP-even Higgs (H), pseudoscalar Higgs (A) and charged Higgs (H^\pm). The *alignment limit*, in which h resembles SM Higgs boson, is naturally achieved in this model [46].

The most general Yukawa Lagrangian involving two generations of VLLs is given by,

$$\begin{aligned} \mathcal{L}_{\text{Yuk}} = & -M_1 \overline{L}'_{L1} L''_{R1} - M_2 \overline{L}'_{L1} L''_{R2} - M_3 \overline{L}'_{L2} L''_{R1} \\ & - M_4 \overline{L}'_{L2} L''_{R2} \\ & - \frac{1}{2} M_5 \overline{\nu}^c_{L1} \nu''_{L1} - \frac{1}{2} M_6 \overline{\nu}^c_{L2} \nu''_{L2} - \frac{1}{2} M_7 \overline{\nu}^c_{R1} \nu'_{R1} \\ & - \frac{1}{2} M_8 \overline{\nu}^c_{R2} \nu'_{R2} - M_9 \overline{\nu}''_{L1} \nu'_{R1} \\ & - M_{10} \overline{\nu}''_{L1} \nu'_{R2} - M_{11} \overline{\nu}''_{L2} \nu'_{R1} - M_{12} \overline{\nu}''_{L2} \nu'_{R2} \end{aligned}$$

$$\begin{aligned} & -M_{L1} \overline{e}''_{L1} e'_{R1} - M_{L2} \overline{e}''_{L2} e'_{R2} \\ & -M_{L3} \overline{e}''_{L1} e'_{R2} - M_{L4} \overline{e}''_{L2} e'_{R1} \\ & -y_2[(\overline{L}'_{L1} \tilde{\phi}_2 + \overline{L}'_{L2} \tilde{\phi}_1) \nu'_{R1} + (\overline{L}'_{L1} \tilde{\phi}_1 - \overline{L}'_{L2} \tilde{\phi}_2) \nu'_{R2}] \\ & -y_4\left[(\overline{L}''_{R1} \tilde{\phi}_2 + \overline{L}''_{R2} \tilde{\phi}_1) \nu''_{L1} \right. \\ & \left. + (\overline{L}''_{R1} \tilde{\phi}_1 - \overline{L}''_{R2} \tilde{\phi}_2) \nu''_{L2}\right] - y'_2\left[(\overline{L}'_{L1} \phi_2 + \overline{L}'_{L2} \phi_1) e'_{R1} \right. \\ & \left. + (\overline{L}'_{L1} \phi_1 - \overline{L}'_{L2} \phi_2) e'_{R2}\right] \\ & -y'_4\left[(\overline{L}''_{R1} \phi_2 + \overline{L}''_{R2} \phi_1) e''_{L1} \right. \\ & \left. + (\overline{L}''_{R1} \phi_1 - \overline{L}''_{R2} \phi_2) e''_{L2}\right] + \text{h.c.} \tag{5} \end{aligned}$$

Here the charge conjugated fields are denoted with superscript “c” in Eq. (5). In presence of exact S_3 -symmetry, the masses of the VLLs will be proportional to the product of Yukawa coupling and the electroweak vacuum expectation value (VEV), which in turn will lead to non-perturbative Yukawa couplings (for vector lepton masses ~ 1 TeV). Thus we introduce Dirac and Majorana mass terms in Eq. (5), that break S_3 -symmetry softly, while the rest of the terms in Eq. (5) are S_3 -symmetric.

Two generations of VLLs comprise of eight neutral and four charged flavor eigenstates. Thus we can construct eight neutral mass eigenstates ($N_i, i = 1-8$) and four charged mass eigenstates ($E_i^\pm, i = 1-4$) out of the aforementioned flavor eigenstates. The unbroken Z_2 symmetry in the model allows the lightest neutral state of the VLLs to act as the DM candidate. It also ensures that the mixing of VLL with SM fermions is also prohibited. We do note that the model can incorporate tiny neutrino masses radiatively through contributions from the Z_2 odd fermions. We however focus on the collider signals of the VLLs at the ILC and leave that study for future considerations. The mass matrices for the neutral and charged fermions and the details of their diagonalisation can be found in [48].

Table 3 Masses of neutral and charged VLLs for four benchmarks

Benchmark points	M_{N_1} (GeV)	M_{N_2} (GeV)	M_{N_3} (GeV)	M_{N_4} (GeV)	M_{N_5} (GeV)	M_{N_6} (GeV)	M_{N_7} (GeV)	M_{N_8} (GeV)	$M_{E_1^\pm}$ (GeV)	$M_{E_2^\pm}$ (GeV)	$M_{E_3^\pm}$ (GeV)	$M_{E_4^\pm}$ (GeV)
BP1	81.3	86.9	119.3	154.4	211.6	268.7	688.4	856.9	171.0	211.8	260.0	322.0
BP2	193.8	204.8	239.8	245.7	268.3	274.9	454.5	494.7	280.2	313.0	356.8	398.5
BP3	261.4	262.5	263.2	263.4	264.0	297.1	444.9	505.5	280.2	313.0	356.7	398.5
BP4	402.8	456.9	461.3	466.1	467.3	508.0	518.3	653.7	486.2	539.4	592.3	657.1

Table 4 DM masses along with DM relic density, spin-dependent, spin-independent cross-sections, thermally averaged indirect detection annihilation cross-sections and corresponding dominant annihilation modes for four benchmarks

Benchmark points	M_{DM} (GeV)	$\Omega_{\text{DM}} h^2$	σ_{SD} cm ²	σ_{SI} cm ²	Annihilation cross-section (for indirect detection only) $\langle \sigma v \rangle$ (cm ³ /s)	Annihilation mode (for indirect detection only)
BP1	81.3	1.04×10^{-1}	3.4×10^{-42}	4.4×10^{-49}	2.41×10^{-28}	$W^+ W^-$ (100%)
BP2	193.8	9.36×10^{-4}	5.98×10^{-42}	2.54×10^{-49}	3.79×10^{-26}	ZZ (53.8%) $W^+ W^-$ (46.1%)
BP3	261.4	4.14×10^{-3}	2.57×10^{-41}	1.06×10^{-46}	2.49×10^{-26}	ZZ (55.5%) $W^+ W^-$ (44.3%)
BP4	402.8	2.97×10^{-4}	7.16×10^{-41}	9.86×10^{-49}	1.05×10^{-26}	ZZ (52.0%) $W^+ W^-$ (46.3%)

3 Collider searches

By the virtue of Z_2 -symmetry, the lightest neutral VLL N_1 cannot decay and becomes a possible DM candidate. To explore the model parameter space compatible with relic density ($\Omega_{\text{DM}} h^2$),¹ direct and indirect DM searches, we implement the model Lagrangian in FeynRules [55] to generate the interaction vertices and mass matrices. The CALCHEP [56] compatible model files obtained from FeynRules is then included in micrOMEGAS [57], which helps us to calculate the DM observables like relic density ($\Omega_{\text{DM}} h^2$), spin-dependent (σ_{SD}) and spin-independent (σ_{SI}) cross-sections, thermally averaged annihilation cross-sections ($\langle \sigma v \rangle$), etc. We choose four representative benchmark points BP1 BP2, BP3 and BP4 according to low, medium and high DM masses, that we found consistent with observed relic abundance obtained from the PLANCK experiment [58], and also allowed by the stringent bounds coming from the direct detection experiments like LUX [59] for spin-independent cross-sections and PICO [60] for spin-dependent cross-sections, and from the indirect detection bounds coming from FERMI-LAT [61], MAGIC [62] and PLANCK [58] experiments. The masses of the neutral (N_i s) and charged (E_i^\pm s) VLLs

¹ Ω_{DM} is defined as the ratio of non-baryonic DM density to the critical density of the universe and h is the reduced Hubble parameter (not to be confused with SM Higgs h).

for our chosen benchmark points can be found in Table 3. All these four benchmark points represent model parameters which satisfy theoretical constraints like stability of the scalar potential, perturbativity and constraints coming from electroweak precision data and Higgs signal strengths.² $\Omega_{\text{DM}} h^2$, σ_{SD} , σ_{SI} , $\langle \sigma v \rangle$ and dominant annihilation modes for indirect detection³ along with corresponding dark matter masses for the aforementioned benchmark points (BPs) are tabulated in Table 4. Our choice of BP's is envisaged to cover varied and complementary features of the model. For example, BP1 corresponds to low DM mass, BP2 corresponds to a slightly heavier DM mass with substantial mass splitting with the charged VLLs, BP3 corresponds to a *compressed spectrum* where the mass difference between the components of the VLL's are ~ 20 GeV while BP4 corresponds to an overall heavy spectrum with higher DM mass which renders them close to threshold value of the ILC center of mass energy.

We focus on the $\sqrt{s} = 1$ TeV of ILC and present our analysis for some specific processes in the S_3 -symmetric model which gives us the semi-leptonic $1\ell + 2j + E/T$, fully leptonic

² More details can be found in our earlier work [48].

³ The 6th and 7th columns of Table 4 actually refer to the $\langle \sigma v \rangle$ relevant for indirect detection, and, the corresponding annihilation channels respectively. The aforementioned indirect detection annihilation cross sections alone cannot lead to an estimate for the relic density since there might be other annihilation/coannihilation channels entering the relic density calculation.

$2\ell + E/T$ and $4\ell + E/T$ ⁴ and the fully hadronic $4j + E/T$ final states. The $1\ell + 2j + E/T$ and $4j + E/T$ channel containing multi-jets prove to be promising signals at the ILC, compared to LHC where huge SM backgrounds would supersede the signal. The spectrum with higher DM mass also proved hard to search at LHC [48] even with high integrated luminosity, since corresponding signal cross-section was too small to yield significant signal significance.

To generate the signal and SM background at leading order (LO), we use the public package MG5aMC@NLO [63]. We first use the following *acceptance cuts*:

$$\begin{aligned} p_T^j &> 20 \text{ GeV}, & |\eta_j| &< 5.0, \\ p_T^\ell &> 10 \text{ GeV}, & |\eta_\ell| &< 2.5, \\ \Delta R_{ij} &> 0.4, & \text{with } i, j = \ell, \text{ jets.} \end{aligned} \tag{6}$$

Here $p_T^{j(\ell)}$, $|\eta_{j(\ell)}|$ are the transverse momentum and pseudo-rapidity of jets (leptons). ΔR_{ij} is defined as: $\Delta R_{ij} = \sqrt{\Delta\eta_{ij}^2 + \Delta\phi_{ij}^2}$, where $\Delta\eta_{ij}$ ($\Delta\phi_{ij}$) is the difference between the pseudo-rapidity (azimuthal angles) of i th and j th particle in the final state. Subsequent decays of the unstable particles are incorporated in Pythia8 [64]. To emulate the detector effects into the analysis, we pass the signal and background events in Delphes-3.4.1 [65] using the default ILD detector simulation card. We note that the results obtained from traditional cut-based analysis are improved further by using Decorrelated Boosted Decision Tree (BDTD) algorithm embedded in TMVA (Toolkit for Multivariate Data Analysis) [66] platform. The signal significance \mathcal{S} can be calculated in both cut-based and multivariate analysis using $\mathcal{S} = \sqrt{2 \left[(S+B) \log \left(\frac{S+B}{B} \right) - S \right]}$, with $S(B)$ denoting the number of signal (background) events surviving the cuts on relevant kinematic variables.

3.1 $2\ell + E/T$ final state

We begin with the leptonic signal consisting of two charged leptons. The final state contains same or different flavour and opposite sign (OS) di-leptons along with E/T . For the benchmark points BP1, BP2 and BP4 dominant contribution to the $2\ell + E/T$ final state comes from $e^+e^- \rightarrow E_1^+E_1^- \rightarrow W^+W^-E/T$ channel, where W^\pm is assumed to decay leptonically. But for BP3, the contribution comes from three body decay, namely $e^+e^- \rightarrow E_1^+E_1^- \rightarrow \ell^+\ell^-E/T$. This is due to the fact that mass difference between E_1^\pm and N_1 is much less than the mass of W^\pm . Here we consider the following processes that can lead to the $2\ell + E/T$ final state:

$$\begin{aligned} e^+e^- &\rightarrow E_i^+E_j^-, E_{i,j}^\pm \rightarrow \ell^\pm N_1, \\ e^+e^- &\rightarrow N_k N_1, N_k \rightarrow \ell^+\ell^- N_1 \end{aligned} \tag{7}$$

where $i, j = 1 \dots 4$ and $k, m = 1 \dots 8$. These processes can give rise to the $2\ell + E/T$ final state depending on the mass spectrum of the VLL's in individual benchmarks. Here we choose the same or different flavour and opposite sign (OS) di-leptons in such a way that the leading and sub-leading leptons have the transverse momenta greater than 10 GeV, i.e. $p_T^{\ell_1, \ell_2} > 10 \text{ GeV}$. At the same time, we reject any third lepton in the final state. Since our signal does not contain any jet, we veto the light jets as well as b jets.

The dominant background comes from the $e^+e^- \rightarrow \ell^+\ell^- + E/T$ final state comprising of the following possible subprocesses that lead to a similar final state:

- $e^+e^- \rightarrow W^+W^-; W^+ \rightarrow \ell^+ \nu_\ell, W^- \rightarrow \ell^- \bar{\nu}_\ell,$
- $e^+e^- \rightarrow ZZ; Z \rightarrow \ell^+\ell^-, Z \rightarrow \nu_\ell \bar{\nu}_\ell,$
- $e^+e^- \rightarrow W^+W^-Z; W^+ \rightarrow \ell^+ \nu_\ell, W^- \rightarrow \ell^- \bar{\nu}_\ell, Z \rightarrow \nu_\ell \bar{\nu}_\ell,$
- $e^+e^- \rightarrow ZZZ; Z \rightarrow \ell^+\ell^-, Z \rightarrow \nu_\ell \bar{\nu}_\ell, Z \rightarrow \nu_\ell \bar{\nu}_\ell.$

A promising feature at the ILC would be the use of polarized beams which can affect specific physics studies in which certain chirality in currents are favored/conserved. To see our signal in the same spirit we calculate the signal and background cross sections corresponding to both polarised ([80% left polarised e^- , 30% right polarised e^+ beam] and [80% right polarised e^- and unpolarised e^+ beam]) and unpolarised e^+e^- beams [67] which are tabulated in Table 5. From now on, we shall only present the distributions and calculate the signal significances for the unpolarised incoming beams using cut-based as well as BDT analysis.

We carry out the cut-based analysis by looking at some relevant kinematic variables which can help design proper cuts (A_1, A_2, A_3) on them to improve the signal over the backgrounds.

- A_1 : We depict the normalized pseudorapidity distributions of the leading and sub-leading leptons in Fig. 1a and b. For the background, the leptons can be produced via s-channel exchange of γ, Z as well as t-channel exchange of ν 's, which results in the peaks at higher η values. However, for the signal, the leptons are produced from the decay of the W^\pm , which are generated from the decay of heavier VLLs, produced via s-channel exchange of γ, Z . As a result, the η distribution for the signal is more centrally peaked. We note that, choosing $|\eta_{l_{1,2}}| < 1.0$ helps to reduce the background significantly.
- A_2 : The normalized distribution of the invariant mass of the opposite sign (OS) lepton pair (same or different flavor) $M_{\ell^+\ell^-}$ is shown in Fig. 1c. Since the $2\ell + E/T$ background consists of the contributions from ZZ and

⁴ Here ℓ represents electron or muon and E/T denotes missing transverse energy.

Table 5 The leading order (LO) effective cross-sections of the signal and background for $2\ell + E/T$ final state at 1 TeV ILC using unpolarised and polarised incoming beams. P_{e^-}, P_{e^+} denotes the polarisation for the e^- and e^+ beam respectively. L and R is used to denote whether the beam is left or right polarised

	Cross section for $(P_{e^-}, P_{e^+} = 0, 0)$ (in fb)	Cross section for $(P_{e^-}, P_{e^+} = 80\%L, 30\%R)$ (in fb)	Cross section for $(P_{e^-}, P_{e^+} = 80\%R, 0)$ (in fb)
Signal benchmarks			
BP1	6.8	11.77	5.11
BP2	5.28	9.49	3.60
BP3	4.42	7.95	3.01
BP4	0.71	1.29	0.47
Background			
$e^+e^- \rightarrow 2\ell + E/T$	420.22	922.3	88.81

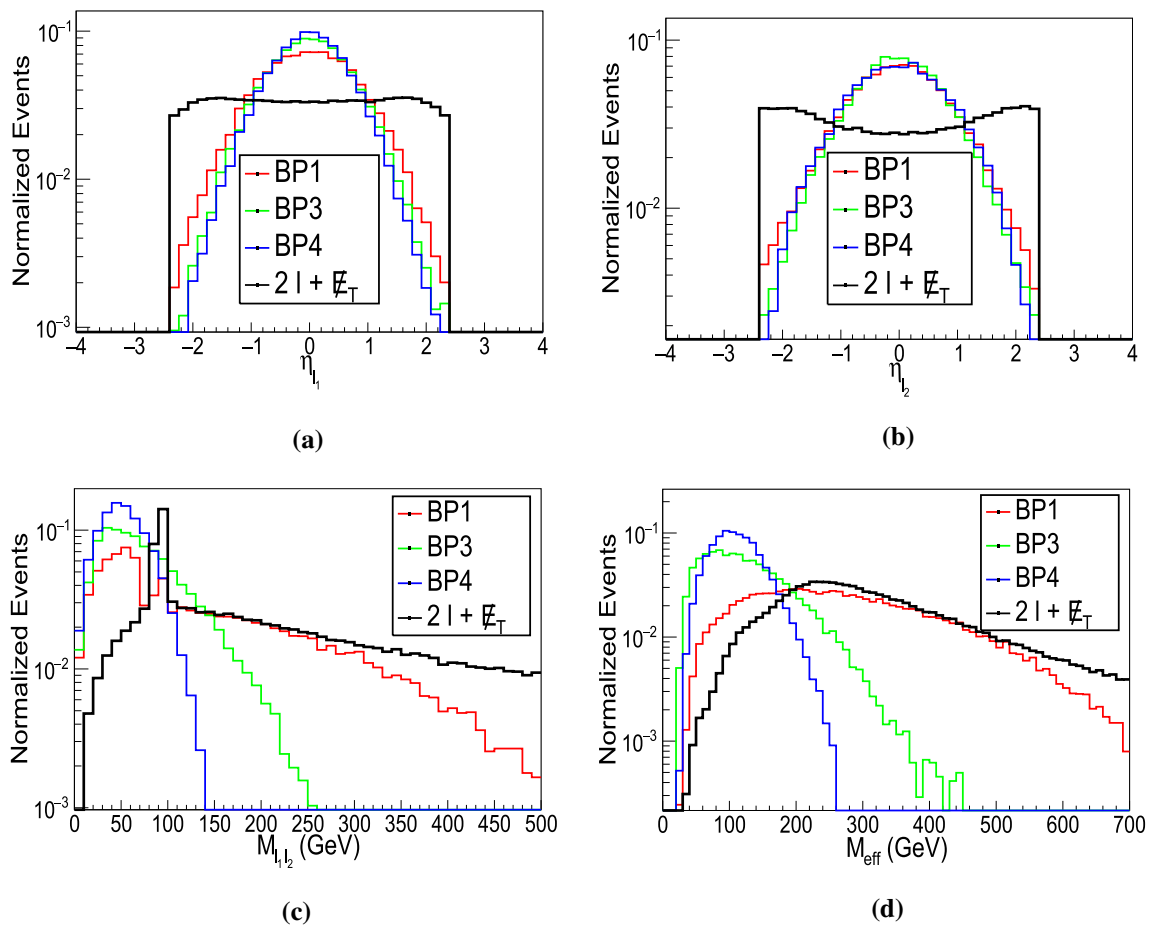


Fig. 1 Normalized distributions of $\eta_{\ell_1}, \eta_{\ell_2}, M_{\ell_1\ell_2}, M_{\text{eff}}$ for $2\ell + E/T$ channel at 1 TeV ILC

γ^*Z , to exclude the Z-peak, we reject events which lie within the window: $|M_{\ell^+\ell^-} - M_Z| < 15$ GeV. At the same time, we also demand $M_{\ell^+\ell^-} > 12$ GeV to reduce the γ^*Z background contribution.

- A_3 : The variable M_{eff} is constructed as the scalar sum of the lepton p_T and E/T . The distribution is shown in Fig. 1d. Instead of giving cuts on the lepton p_T and E/T separately, it is useful to put a cut on M_{eff} which helps to reject the background more efficiently. Since for BP3

and BP4, the mass difference between the charged and neutral component of the VLL's are smaller compared to BP1 and BP2, the lepton p_T is less. As a result, M_{eff} peaks at a smaller value for BP3 and BP4. We impose an upper cut: $M_{\text{eff}} < 500$ (350) GeV for BP1 and BP2 (BP3 and BP4) to reduce the background.

We tabulate the number of signal and background events surviving after the application of each cut for each benchmark

Table 6 The cut-flow for signal and backgrounds for $2\ell + E/T$ channel along with the required integrated luminosity required for 5σ significance for benchmarks BP1, BP2, BP3 and BP4 at 1 TeV ILC. The bracketed term in the A_3 cut denotes the surviving number of events for $M_{\text{eff}} < 350$ GeV cut for the background

SM-background	Number of events after cuts ($\mathcal{L} = 100 \text{ fb}^{-1}$)			$\mathcal{L}_{5\sigma}$ (fb^{-1})
	A_1	A_2	A_3	
$2\ell + E/T$	4826	2817	535 (289)	
Signal				
BP1	417	366	318	16
BP2	322	261	260	23
BP3	291	225	223	18
BP4	45	36	36	570

at an integrated luminosity 100 fb^{-1} in Table 6. From Table 6 we infer that to attain 5σ significance, we need 16 fb^{-1} , 23 fb^{-1} , 18 fb^{-1} and 570 fb^{-1} integrated luminosity ($\mathcal{L}_{5\sigma}$) for BP1, BP2, BP3 and BP4 respectively.

$$S_{\text{sys}} = \sqrt{2 \left((N_S + N_B) \log \left(\frac{(N_S + N_B)(N_B + \sigma_B^2)}{N_B^2 + (N_S + N_B)\sigma_B^2} \right) - \frac{N_B^2}{\sigma_B^2} \log \left(1 + \frac{\sigma_B^2 N_S}{N_B(N_B + \sigma_B^2)} \right) \right)}, \tag{9}$$

To showcase further improvement of the signal sensitivity from the cut-based analysis, we carry out the multivariate analysis (MVA) using *Decorrelated Boosted Decision Tree (BDTD)* algorithm within the Toolkit for Multivariate Data Analysis (TMVA) framework. A detailed description of the method has already been described in one of our earlier work [48]. According to the discerning ability between the signal and the backgrounds of this channel, the most important kinematic variables turn out to be ⁵:

$$M_{\ell_1 \ell_2}, \eta_{\ell_1}, \eta_{\ell_2}, E/T, M_{\text{eff}}, p_T^{\ell_1}. \tag{8}$$

The BDTD parameters like `NTrees`, `MinNodeSize`, `MaxDepth`, `nCuts` and `KS-scores` [48] for both signal and backgrounds are tabulated in Table 7. The first four input parameters are regulated in such a way, that the `KS-scores` for both signal and backgrounds become stable [48]. The next task is to tune the *BDT cut value* or *BDT score* to maximise the signal significance. Figure 2b shows the variation of significance with BDT-score. From this figure, it is evident that the signal significances of different benchmarks attain a maximum value for different BDT cut values. The BDT scores for BP1, BP2, BP3 and BP4 are 0.167, 0.164, 0.23 and 0.201 respectively. In the *Receiver’s Operative Characteristic (ROC)* plot (Fig. 2a), we show the degree of background

rejection against signal efficiency. It can clearly be inferred that the degree of background rejection is maximum for BP4 (magenta curve in Fig. 2(a)).

The signal and background yields for $2\ell + E/T$ channel at $\mathcal{L} = 100 \text{ fb}^{-1}$ along with the integrated luminosity required to achieve a 5σ significance for each benchmark points using MVA, have been tabulated in Table 8. The integrated luminosities required for achieving 5σ significance for BP1, BP2, BP3, BP4 are 17.1, 22.8, 14.5, 216.3 respectively. Comparing with the results obtained from the cut-based analysis, one can find that the integrated luminosities required for achieving 5σ significance is lowered for BP3 and BP4 after performing the BDTD analysis, which implies an overall improvement of results after the multivariate analysis is done. It is instructive to acknowledge systematic uncertainties at the experiment which can effect our results. To show this we include a 5% systematic uncertainty and highlight its effect in Table 8 along side the null systematic uncertainty results. The signal significance gets modified by introducing a systematic uncertainty ($\sigma_{\text{sys_un}}$) in the SM background estimation [68] following:

where $\sigma_B = \sigma_{\text{sys_un}} \times N_B$.

3.2 $1\ell + 2j + E/T$ final state

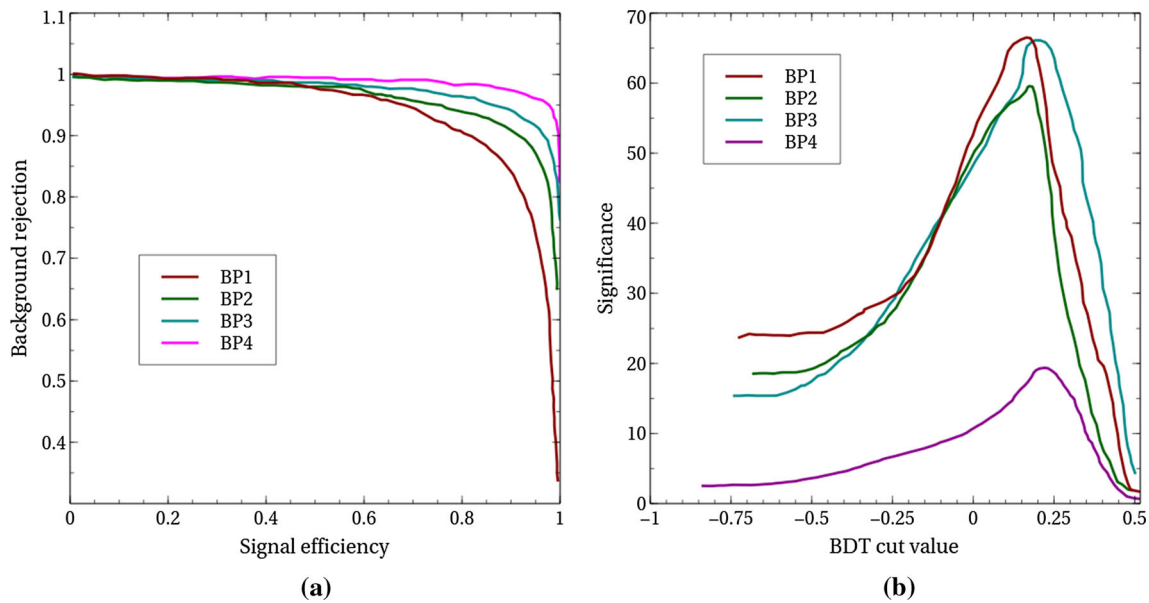
The dominant contribution to $1\ell + 2j + E/T$ final state originates from $e^+e^- \rightarrow E_1^+ E_1^- \rightarrow W^+ W^- E/T$, where one of the W^\pm decays leptonically and other one decays hadronically. The SM processes that can give rise to the similar final state are:

- $e^+e^- \rightarrow W^+W^-; W^+(W^-) \rightarrow \ell^+(\ell^-) \nu_\ell(\bar{\nu}_\ell), W^-(W^+) \rightarrow jj,$
- $e^+e^- \rightarrow ZZ; Z \rightarrow \ell^+\ell^-, Z \rightarrow jj,$ (one of the leptons is missed)
- $e^+e^- \rightarrow W^+W^-Z;$
 1. $W^+ \rightarrow \ell^+ \nu_\ell, W^- \rightarrow \ell^- \bar{\nu}_\ell, Z \rightarrow jj,$ (one of the leptons is missed)
 2. $W^+ \rightarrow \ell^+ \nu_\ell, W^- \rightarrow jj, Z \rightarrow \nu_\ell \bar{\nu}_\ell,$
- $e^+e^- \rightarrow ZZZ; Z \rightarrow \ell^+\ell^-, Z \rightarrow jj, Z \rightarrow \nu_\ell \bar{\nu}_\ell,$ (one of the leptons is missed)
- $e^+e^- \rightarrow Zh;$
 1. $Z \rightarrow \ell^+\ell^-, h \rightarrow jj$ (one of the leptons is missed)
 2. $Z \rightarrow jj, h \rightarrow \ell^+\ell^-$ (one of the leptons is missed)

⁵ This is clearly in accordance with the variables highlighted in the cut-based analysis.

Table 7 Tuned BDT parameters for BP1, BP2, BP3 and BP4 for the $2\ell + E_T$ channel

	NTrees	MinNodeSize (%)	MaxDepth	nCuts	KS-score for Signal (Background)
BP1	110	4	2.0	40	0.545 (0.437)
BP2	110	4	2.0	50	0.303 (0.418)
BP3	110	3	2.0	50	0.969 (0.053)
BP4	110	3	2.0	50	0.018 (0.035)

**Fig. 2** (a) ROC curves for chosen benchmark points for $2\ell + E_T$ channel. (b) BDT-scores corresponding to BP1, BP2, BP3 and BP4 for $2\ell + E_T$ channel**Table 8** The signal and background yields at 1 TeV ILC with 100 fb^{-1} integrated luminosity for BP1, BP2, BP3 and BP4 along with luminosity required for 5σ significance for the $e^+e^- \rightarrow 2\ell + E_T$ channel after performing the BDT analysis

Benchmark point	Signal yield at 100 fb^{-1}	Background yield at 100 fb^{-1}	Significance at 100 fb^{-1} with 0%(5%) systematic uncertainty	$\mathcal{L}_{5\sigma}$ (fb^{-1}) with 0%(5%) systematic uncertainty
BP1	346	711	12.1 (6.9)	17.1 (52.5)
BP2	283	643	10.5 (6.7)	22.8 (55.7)
BP3	214	203	13.1 (10.2)	14.5 (24.0)
BP4	50	200	3.4 (2.7)	216.3 (342.9)

Contributions from ZZZ and Zh backgrounds are insignificant due to small production rate. The LO cross sections of the signal and backgrounds using polarised and unpolarised incoming beams are tabulated in Table 9.

Since the signal consists of one lepton and two jets along with transverse missing energy, we reject any second lepton or any third jet in the final state for the backgrounds. This helps us to suppress ZZ background. Finally we are left with W^+W^- and W^+W^-Z background. Apart from the basic acceptance cuts mentioned in Eq. (6), we implement the following cuts to enhance the signal over backgrounds.

- B_1 : The pseudorapidity distributions for lepton and jets are different for the signal and background as can be seen in Fig. 3a–c due to the t-channel dominant background. Choosing the pseudo-rapidity of the lepton and jets within the range: $|\eta_{\ell_1}|, |\eta_{j_{1,2}}| < 1.0$, helps to reduce the background drastically.
- B_2 : The normalized E_T distribution is shown in Fig. 3d. For the background, the missing energy comes from the neutrinos and the distribution peaks at a lower E_T value. On the other hand, for the signal, apart from the neutrinos, missing energy can arise from the DM candidates and as

Table 9 The effective cross-sections of the signal and backgrounds for $1\ell + 2j + E/T$ channel at LO at 1 TeV ILC using unpolarised and polarised incoming beams

	Cross section for $(P_{e^-}, P_{e^+} = 0, 0)$ (in fb)	Cross section for $(P_{e^-}, P_{e^+} = 80\%L, 30\%R)$ (in fb)	Cross section for $(P_{e^-}, P_{e^+} = 80\%R, 0)$ (in fb)
Signal benchmarks			
BP1	19.30	33.39	14.50
BP2	17.27	31.04	11.76
BP3	9.11	16.36	6.20
BP4	1.65	3.0	1.10
Background subprocesses			
$e^+e^- \rightarrow W^+W^-$	229.21	535.74	33.08
$e^+e^- \rightarrow ZZ$	3.41	5.77	2.65
$e^+e^- \rightarrow W^+W^-Z$	3.82	8.89	0.57
$e^+e^- \rightarrow ZZZ$	0.01	0.02	0.009
$e^+e^- \rightarrow Zh$	0.18	0.27	0.27

a result it will peak relatively at a higher value. A lower cut of $E/T > 50$ GeV helps to diminish the background.

- B_3 : We use the kinematic variable transverse mass M_T ⁶ to distinguish the signal and background. As expected for the background, M_T will peak at the W^\pm mass while for the signal the corresponding distribution is smeared as seen in Fig. 3e. As there is additional source of E/T in the signal, we get a tail in M_T distribution for the signal. We observe that putting a cut of $M_T > 90$ GeV helps to suppress the background.
- B_4 : We depict the $\Delta R_{\ell_1 j_{1,2}}$ distributions in Fig. 4a, b. It can be seen that an upper cut of $\Delta R_{\ell_1 j_{1,2}} < 3.2$ helps to enhance the signal significance.

We show the effect of the each cut in Table 10. It is noticed that after putting all the cuts, we merely need 4, 3 and 14 fb^{-1} integrated luminosity to probe BP1, BP2 and BP3 for achieving 5σ significance. However, due to small production cross-section, to probe BP4 we need comparatively higher (220fb^{-1}) luminosity.

We now perform the multivariate analysis for $1\ell + 2j + E/T$ channel. According to the degree of differentiating potential between the signal and backgrounds, the most important variables turn out to be:

$$\Delta R_{\ell_1 j_1}, \Delta R_{\ell_1 j_2}, M_T, E/T, \eta_{\ell_1}, \eta_{j_1}, \eta_{j_2}, M_{j_1 j_2}, \Delta\phi_{\ell_1 j_1}, \Delta\phi_{\ell_1 j_2} \tag{10}$$

Here $\Delta\phi_{\ell_1 j_1}$, ($\Delta\phi_{\ell_1 j_2}$) are the azimuthal angle between ℓ_1 and j_1 (j_2), while the other variables have been defined earlier. The tuned BDT parameters for each benchmark points

⁶ M_T is defined as $M_T = \sqrt{2p_T^\ell E/T (1 - \cos \Delta\phi_{\ell, E/T})}$, where $\Delta\phi_{\ell, E/T}$ is the azimuthal angle between the lepton and transverse missing energy.

are listed in Table 11. The signal and background yields for an integrated luminosity 100fb^{-1} are shown in Table 12. The same table contains the necessary integrated luminosities to attain 5σ significance for all benchmarks. Fig. 5a and b depict the ROC curves and variation of significances with BDT-scores for all benchmarks respectively. The BDT scores for the four benchmarks are 0.13, 0.165, 0.193, 0.141 respectively.

3.3 $4\ell + E/T$ final state

In this section, we analyse the final state comprising $4\ell + E/T$. The $4\ell + E/T$ final state for the signal can be obtained from the following processes:

$$e^+e^- \rightarrow N_i N_i, N_i \rightarrow N_1 \ell^+ \ell^-, \tag{11}$$

with $i = 2, 3, \dots 8$.

Table 10 The cut-flow for signal and backgrounds along with the significances for BP1, BP2, BP3 and BP4 at 1 TeV ILC and the required integrated luminosity for 5σ significance for the $e^+e^- \rightarrow 1\ell + 2j + E/T$ channel

SM-background	Number of events after cuts ($\mathcal{L} = 100 \text{fb}^{-1}$)				
	B_1	B_2	B_3	B_4	
W^+W^-	1008	873	39	26	
W^+W^-Z	101	85	33	28	
Signal					$\mathcal{L}_{5\sigma}$ (fb^{-1})
BP1	1129	891	329	310	4
BP2	915	710	330	314	3
BP3	526	334	134	127	14
BP4	108	42	28	27	220

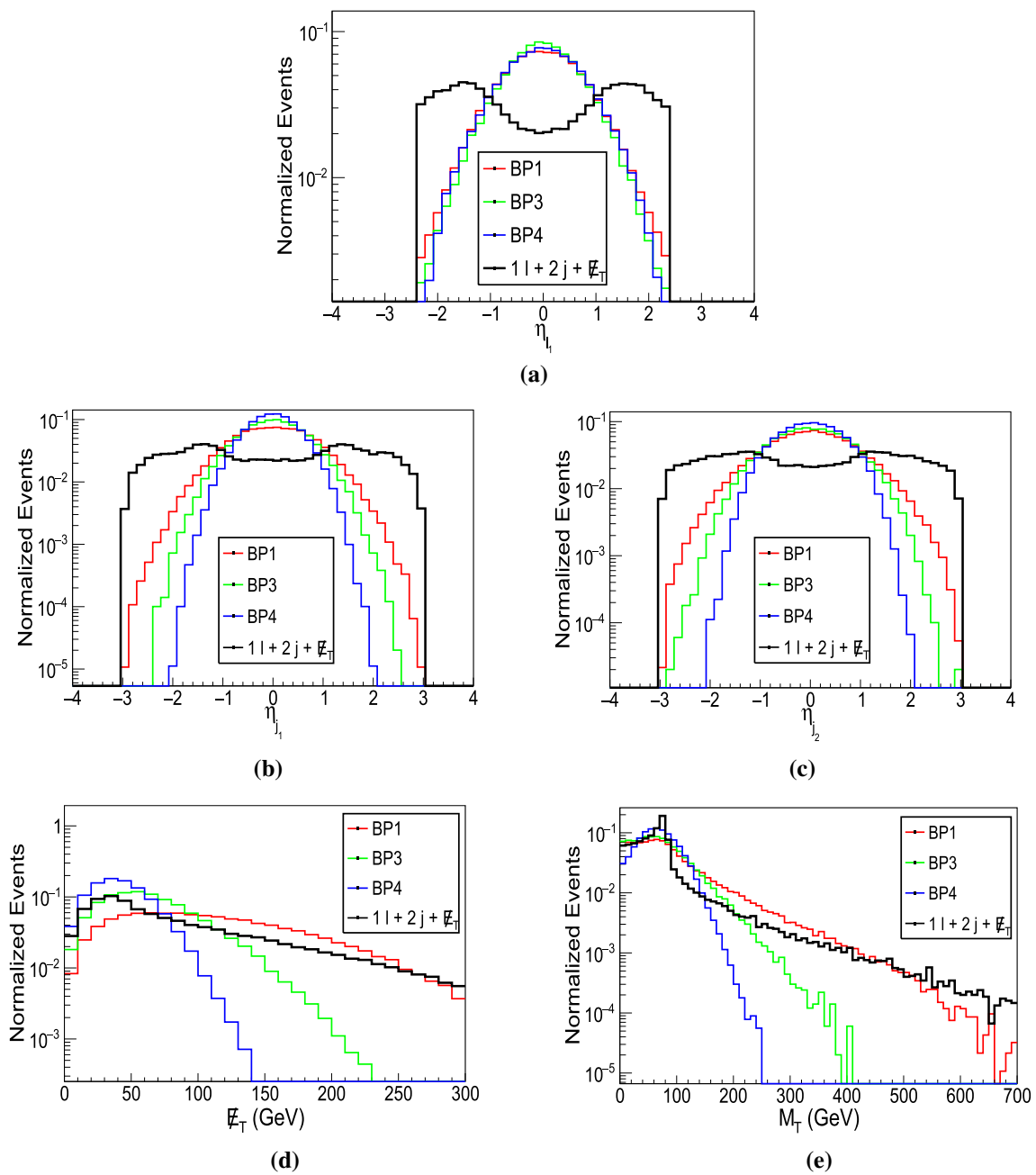


Fig. 3 Normalized distributions of η_{ℓ_1} , η_{j_1} , η_{j_2} , E_T , M_T for $1\ell + 2j + E_T$ channel at 1 TeV ILC

Table 11 Tuned BDT parameters for BP1, BP2, BP3 and BP4 for the $1\ell + 2j + E_T$ channel

	NTrees	MinNodeSize (%)	MaxDepth	nCuts	KS-score for Signal (Background)
BP1	110	3	2.0	50	0.263 (0.048)
BP2	110	3	2.0	50	0.576 (0.242)
BP3	110	4	2.0	50	0.071 (0.197)
BP4	110	3	2.0	50	0.809 (0.307)

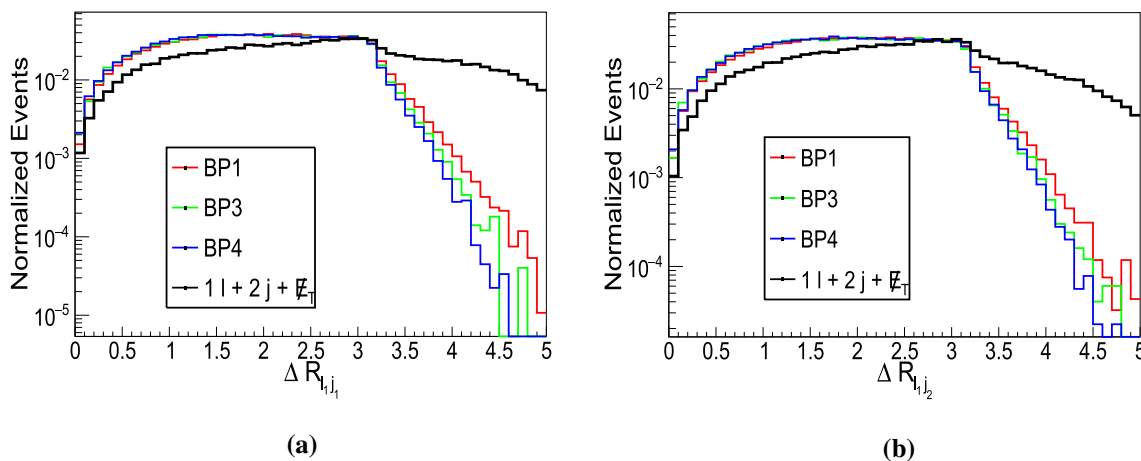


Fig. 4 Normalized distributions of $\Delta R_{l_1 j_1}$, $\Delta R_{l_1 j_2}$ for $1\ell + 2j + E_T$ channel at 1 TeV ILC

Table 12 The signal and background yields at 1 TeV ILC with 100 fb^{-1} integrated luminosity for BP1, BP2, BP3 and BP4 along with luminosity required for 5σ significance for the $e^+e^- \rightarrow 1\ell + 2j + E_T$ channel after performing the BDTD analysis

Benchmark point	Signal yield at 100 fb^{-1}	Background yield at 100 fb^{-1}	Significance at 100 fb^{-1} with 0%(5%) systematic uncertainty	$\mathcal{L}_{5\sigma}$ (fb^{-1}) with 0%(5%) systematic uncertainty
BP1	1531	641	47.3 (25.4)	1.1 (3.9)
BP2	1480	301	58.0 (40.3)	0.7 (1.5)
BP3	834	224	40.2 (28.5)	1.5 (3.1)
BP4	151	41	17.0 (15.6)	8.6 (10.3)

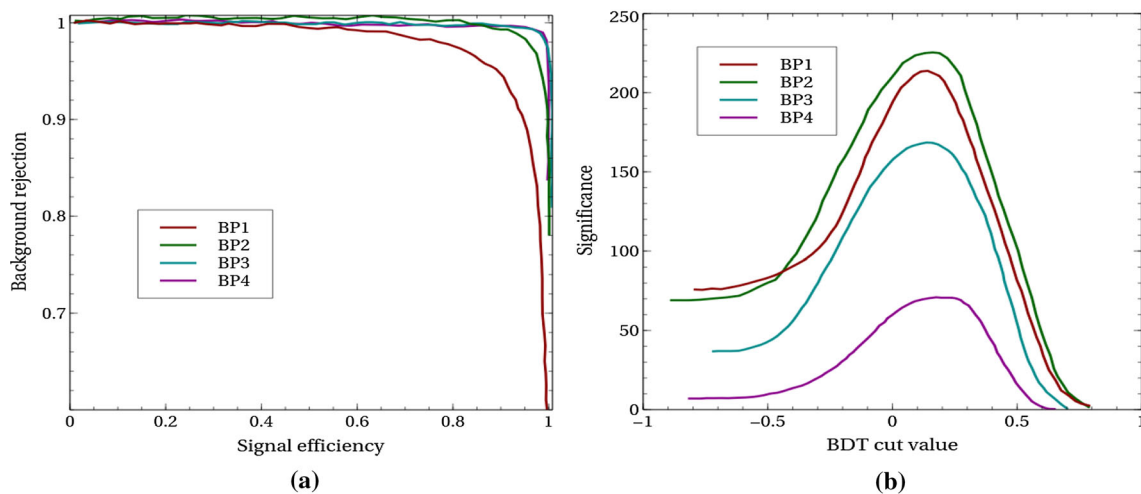


Fig. 5 **a** ROC curves for chosen benchmark points for $1\ell + 2j + E_T$ channel. **b** BDT-scores corresponding to BP1, BP2, BP3 and BP4 for $1\ell + 2j + E_T$ channel

The SM backgrounds [52] that give rise to the similar final state is VVV , ($V = W^\pm, Z$) production along with additional contribution coming from ZZ production. Demanding that opposite sign same flavor (OSSF) lepton pair invariant mass lies away from the Z peak reduces the $ZZ \rightarrow 4\ell$

and ZZZ background significantly. Finally we are left with the irreducible W^+W^-Z background. The signal and background cross sections at LO are depicted in Table 13.

Along with the basic cuts (Eq. (6)), we implement the following cuts to maximise the signal significance:

Table 13 The effective cross-sections of the signal and background for $4\ell + E/T$ signal at LO at 1 TeV ILC using unpolarised and polarised incoming beams

	Cross section for ($P_{e^-}, P_{e^+} = 0, 0$) (in fb)	Cross section for ($P_{e^-}, P_{e^+} = 80\%L, 30\%R$) (in fb)	Cross section for ($P_{e^-}, P_{e^+} = 80\%R, 0$) (in fb)
Signal benchmarks			
BP1	0.029	0.05	0.02
BP2	0.056	0.1	0.038
BP3	0.006	0.01	0.004
BP4	0.001	0.002	0.0007
Background			
$e^+e^- \rightarrow W^+W^-Z$	0.19	0.44	0.029

Table 14 The cut-flow for signal and backgrounds for BP1, BP2, BP3 and BP4 at 1 TeV ILC and the required integrated luminosity for 5σ significance for the $e^+e^- \rightarrow 4\ell + E/T$ channel. The bracketed term in C_4 cut denotes the surviving number of events for $M_{\text{eff}} < 500$ GeV cut for the background

	Number of events after cuts ($\mathcal{L} = 4 \text{ ab}^{-1}$)				$\mathcal{L}_{5\sigma}$ (fb $^{-1}$)
	C_1	C_2	C_3	C_4	
SM-background					
W^+W^-Z	81	35	32	5(2)	
Signal					
BP1	95	69	63	55	550
BP2	188	132	110	109	150
BP3	26	19	10	10	4500
BP4	3	3	2	2	65000

- C_1 : Out of the four leptons, we choose two pairs of OS same flavor leptons ($(M_{\ell+\ell^-})_{1,2}$) which have invariant mass close to the Z -mass. We reject all events where $|(M_{\ell+\ell^-})_{1,2} - M_Z| < 15$ GeV to exclude the Z -peak of ZZ -background.
- C_2 : The pseudo-rapidity distributions of the leading and sub-leading leptons look similar to Fig. 1a, b as the t -channel contribution dominates. The $|\eta_{\ell_{1,2}}| < 1.0$ cut helps to suppress the background.

- C_3 : The E/T distribution for the background peaks at a lower value as it gets contribution only from neutrinos unlike the signal that also gets contribution from the heavy dark matter. A lower cut on $E/T > 30$ GeV helps to enhance the signal significance.
- C_4 : The normalized M_{eff} distribution is similar to Fig. 1d, except a larger tail. This is due to the fact that instead of two leptons, here M_{eff} includes the scalar sum of four lepton p_T 's and the missing transverse energy. We have optimized $M_{\text{eff}} < 600(500)$ GeV for BP1(rest of the BPs) to suppress the background significantly.

We tabulate the surviving events for the signal and backgrounds after each cut in Table 14 at an integrated luminosity 4 ab^{-1} . It can be seen that to probe benchmark BP1 and BP2 at 5σ significance, we need 550 fb^{-1} and 150 fb^{-1} luminosity and BP3 and BP4 are beyond the ILC projected luminosity [49,50].

3.4 $4j + E/T$ final state

This final state originates from $e^+e^- \rightarrow E_1^+E_1^- \rightarrow W^+W^-E/T$ process, where both the W^\pm decay hadronically. The background for this process comes from $e^+e^- \rightarrow$

Table 15 The effective cross-sections of the signal and background for $4j + E/T$ channel at LO at 1 TeV ILC using unpolarised and polarised incoming beams

	Cross section for ($P_{e^-}, P_{e^+} = 0, 0$) (in fb)	Cross section for ($P_{e^-}, P_{e^+} = 80\%L, 30\%R$) (in fb)	Cross section for ($P_{e^-}, P_{e^+} = 80\%R, 0$) (in fb)
Signal benchmarks			
BP1	20.21	34.97	15.18
BP2	18.82	33.66	12.75
BP3	7.21	12.95	4.91
BP4	1.20	2.19	0.80
Background			
$e^+e^- \rightarrow 4j + E/T$	267.69	594.57	77.69

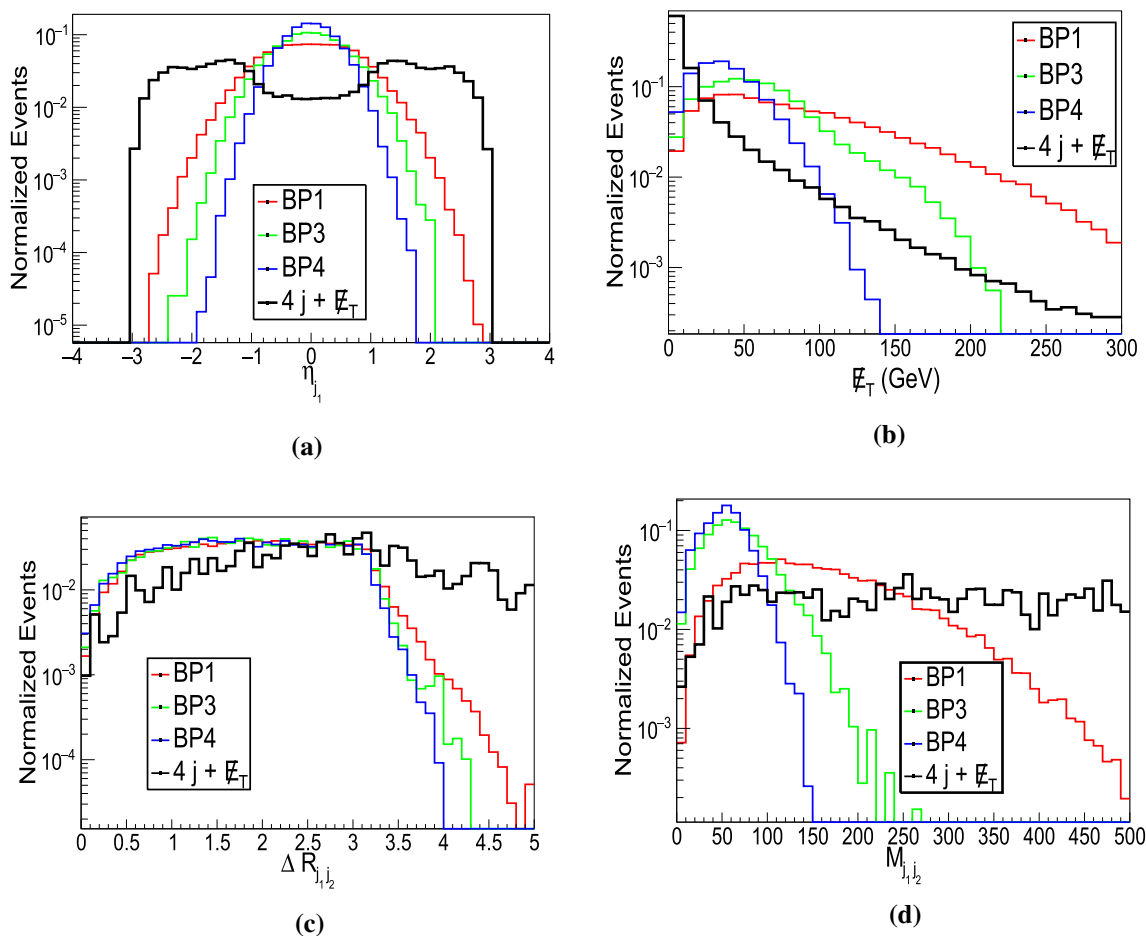


Fig. 6 Normalized distributions of η_{j_1} , E_T , $\Delta R_{j_1 j_2}$, $M_{j_1 j_2}$ for $4j + E_T$ channel at 1 TeV ILC

Table 16 The cut-flow for signal and backgrounds for $4j + E_T$ channel with the required integrated luminosity required for 5σ significance for benchmarks BP1, BP2, BP3 and BP4 at 1 TeV ILC. The

bracketed term in the D_4 cut denotes the surviving number of events for $M_{j_1 j_2} < 150$ GeV cut for the background

SM-background	Number of events after cuts ($\mathcal{L} = 100 \text{ fb}^{-1}$)					
	D_1	D_2	D_3	D_4	Significance at 100 fb^{-1} with 0%(5%) uncertainty	$\mathcal{L}_{5\sigma}$ (fb^{-1}) with 0%(5%) uncertainty
$4j + E_T$	3554	1198	326	134(27)		
Signal						
BP1	1263	1096	1009	921	50.1 (37.9)	1.0 (1.7)
BP2	1224	1058	990	989	52.8 (39.8)	0.9 (1.6)
BP3	507	407	382	370	37.3 (33.7)	1.8 (2.2)
BP4	106	66	63	63	9.5 (9.0)	27.7 (30.9)

$4j + E_T$ which is dominated by di-boson (in that part of the phase space where E_T measurement is not important) and tri-boson production. However, due to small cross-section, ZZZ contributes insignificantly, while W^+W^- , ZZ and W^+W^-Z act as the irreducible backgrounds for this signal. We have demanded a b -veto to reduce the $t\bar{t}$ background ($t\bar{t}$ production cross-section is one order of magnitude less

than ZZ production cross-section and two orders of magnitude less than W^+W^- production cross-section) as the efficiency of mistagging a b jet as light jet is 1%. The effective cross-sections for the signal and backgrounds are shown in Table 15.

To ensure that our signal contains exactly four jets, we veto any fifth jet with $p_T^j > 20$ GeV along with the basic

Table 17 Required integrated luminosity for 5σ significance reach based on cut-based analysis for the chosen benchmark points for $2\ell + E/T$, $1\ell + 2j + E/T$, $4\ell + E/T$, $4j + E/T$ respectively

Benchmark points	$\mathcal{L}_{5\sigma}$ (fb $^{-1}$)			
	$2\ell + E/T$	$1\ell + 2j + E/T$	$4\ell + E/T$	$4j + E/T$
BP1	16	4	550	1.0
BP2	23	3	150	0.9
BP3	18	14	4500	1.8
BP4	570	220	$> 10^4$	27

cuts described in Eq. (6). In addition to these cuts, we put the following set of cuts to suppress the background.

- D_1 : We draw normalized pseudo-rapidity distribution in Fig. 6a for the leading jet. For the signal, the jets are much more centralised. Therefore putting a cut of $|\eta_j| < 1.2$, $j = 1 \dots 4$, helps to suppress the background very efficiently.
- D_2 : For the background, the source of E/T is only the neutrinos coming from the decay of W^\pm or Z . For the signal, the additional source is the massive dark matter. By examining the distribution as depicted in Fig. 6b, we put a cut of $E/T > 30$ GeV to enhance the signal.
- D_3 : ΔR between the jets become an important variable. We put a cut of $\Delta R_{j,ik} < 3.5$, $i \neq k = 1 \dots 4$, to suppress the background.
- D_4 : The invariant mass for two jet pair becomes an efficient variable. For BP1 and BP2, since the mass difference between the charged and neutral VLL's is higher compared to BP3 and BP4, the invariant mass distribution has a larger tail. As seen from Fig. 6d, $M_{j,ik} < 300(150)$ GeV, $i \neq k = 1 \dots 4$, helps to enhance the signal for benchmark BP1 and BP2 (BP3 and BP4) over the background.

We present the cut-flow for the signal and backgrounds at integrated luminosity 100 fb^{-1} in Table 16. We observe that compared to all the remaining aforementioned channels, this channel performs the best.

As we can achieve 5σ significance with low integrated luminosity with cut-based analysis already, we refrain ourselves in performing the multivariate analysis. Comparing with the previous channels, this channel fares the best among all at 1 TeV ILC.

We conclude this section by a thorough comparison of the four aforementioned channels. We have quoted the required luminosity to probe the benchmark points with 5σ significance by cut-based analysis only. From Table 17, it can be seen that out of the four channels, $4j + E/T$ channel performs the best as it requires $< 2 \text{ fb}^{-1}$ luminosity to probe the first three BP's and 27.7 fb^{-1} luminosity to probe BP4 with 5σ significance. $1\ell + 2j + E/T$ channel performs the second best to probe the selected benchmarks. The benchmark

points BP1, BP2, BP3 and BP4 can be probed with 5σ significance with luminosity 4, 3, 14 and 220 fb^{-1} respectively in this mode. The third best performing channel is $2\ell + E/T$. To probe the first three benchmark points with 5σ significance one requires luminosity $< 25 \text{ fb}^{-1}$. However, due to small effective cross-section, probing the BP4 at 5σ , one requires 570 fb^{-1} luminosity. The $4\ell + E/T$ channel performs the worst at ILC although the background cross-sections are small. This is due to the fact that the effective production-cross section of signals in $4\ell + E/T$ channel is very small. Only for BP1 and BP2, 5σ significance can be achieved with 500 fb^{-1} and 150 fb^{-1} integrated luminosity respectively. Thus one can conclude that, the final states containing one or more jets, which are challenging to probe at LHC due to large backgrounds, turn out to be promising at ILC due to clean environment. We would like to mention here that these results can be improved by using the multivariate analysis.

4 Conclusion

In this work we study the signals for an S_3 -symmetric 2HDM extended with two generations of VLLs. We impose an additional Z_2 -symmetry through which the mixing between the SM fermions and VLLs is disallowed, since the SM fermions are even and the VLLs are odd under the aforementioned symmetry. Thus the lightest neutral VLL turns out to be a viable DM candidate owing to the Z_2 -symmetry.

We choose four representative benchmark points BP1, BP2, BP3 and BP4 corresponding to low, medium and high DM masses, which satisfy the constraints coming from vacuum stability, perturbative unitarity, electroweak precision variables and Higgs signal strength along with the DM constraints coming from relic density, direct and indirect detections. We have presented detailed collider analysis for four distinct channels to probe these BPs at 1 TeV ILC, namely $2\ell + E/T$, $1\ell + 2j + E/T$, $4\ell + E/T$ and $4j + E/T$.

For $2\ell + E/T$ and $1\ell + 2j + E/T$ channels, we perform both cut-based and BDT analysis. All these channels originate from the pair production of the charged and neutral VLLs. In the $2\ell + E/T$ channel, both the W^\pm decay leptonically and in the $1\ell + 2j + E/T$ channel, one W^\pm decays leptonically and the other hadronically and for $4j + E/T$ channel, both

the W^\pm decay hadronically. However, it is seen that one can probe $4j + E/T$ channel with 5σ significance with integrated luminosity $< 2 \text{ fb}^{-1}$ for the first 3 benchmark points and with 27 fb^{-1} luminosity for BP4 even with the cut-based analysis. This is the best performing channel at 1 TeV ILC. $1\ell + 2j + E/T$ channel at 1 TeV ILC is the second best performing channel as it requires only $\mathcal{O}(1) \text{ fb}^{-1}$ luminosity to probe the first three benchmark points and 8.6 fb^{-1} luminosity to probe BP4 using MVA. The third well-performing channel is $2\ell + E/T$, where 5σ significance is achieved for the first three BPs with luminosity $< 25 \text{ fb}^{-1}$. However, due to small effective cross-section, one requires 216.3 fb^{-1} luminosity to attain 5σ significance for BP4. The $4\ell + E/T$ channel performs the worst among all channels at ILC. Only for BP1 and BP2 with luminosity 550 fb^{-1} and 150 fb^{-1} respectively, one can attain 5σ significance. We find that a better sensitivity to heavier VLLs with high DM masses can be obtained at ILC in both the leptonic and hadronic channels, which proved more challenging and nearly impossible at HL-LHC due to smaller signal cross sections as well as large hadronic backgrounds. Thus ILC will prove to be a better hunting ground for such particles which have electroweak strength interactions.

Acknowledgements IC acknowledges support from DST, India, under grant number IFA18-PH214 (INSPIRE Faculty Award). NG and SKR would like to acknowledge support from the Department of Atomic Energy, Government of India, for the Regional Centre for Accelerator-based Particle Physics (RECAPP).

Data Availability Statement This manuscript has no associated data or the data will not be deposited. [Authors' comment: The data we used in our manuscript to compare with our model estimations are already public from the ATLAS, CMS, LUX, PANDAX-II, Xenon-1T, PICO, FERMI-LAT, MAGIC, PLANCK experiments.]

Open Access This article is licensed under a Creative Commons Attribution 4.0 International License, which permits use, sharing, adaptation, distribution and reproduction in any medium or format, as long as you give appropriate credit to the original author(s) and the source, provide a link to the Creative Commons licence, and indicate if changes were made. The images or other third party material in this article are included in the article's Creative Commons licence, unless indicated otherwise in a credit line to the material. If material is not included in the article's Creative Commons licence and your intended use is not permitted by statutory regulation or exceeds the permitted use, you will need to obtain permission directly from the copyright holder. To view a copy of this licence, visit <http://creativecommons.org/licenses/by/4.0/>.
Funded by SCOAP³.

References

- ATLAS collaboration, G. Aad et al., Observation of a new particle in the search for the Standard Model Higgs boson with the ATLAS detector at the LHC. *Phys. Lett. B* **716**, 1–29 (2012). <https://doi.org/10.1016/j.physletb.2012.08.020>. arXiv:1207.7214
- CMS collaboration, S. Chatrchyan et al., Observation of a new boson at a mass of 125 GeV with the CMS experiment at the LHC. *Phys. Lett. B* **716**, 30–61 (2012). <https://doi.org/10.1016/j.physletb.2012.08.021>. arXiv:1207.7235
- J.L. Rosner, Splitting between up type and down type quark masses via mixing with exotic fermions in E_6 . *Phys. Rev. D* **61**, 097303 (2000). <https://doi.org/10.1103/PhysRevD.61.097303>
- K. Das, T. Li, S. Nandi, S.K. Rai, A new proposal for diphoton resonance from E_6 motivated extra $U(1)$. arXiv:1607.00810
- A. Joglekar, J.L. Rosner, Searching for signatures of E_6 . *Phys. Rev. D* **96**, 015026 (2017). arXiv:1607.06900
- K. Das, T. Li, S. Nandi, S.K. Rai, New signals for vector-like down-type quark in $U(1)$ of E_6 . *Eur. Phys. J. C* **78**, 35 (2018). <https://doi.org/10.1140/epjc/s10052-017-5495-0> arXiv:1708.00328
- T. Moroi, Y. Okada, Radiative corrections to Higgs masses in the supersymmetric model with an extra family and antifamily. *Mod. Phys. Lett. A* **7**, 187–200 (1992). <https://doi.org/10.1142/S0217732392000124>
- T. Moroi, Y. Okada, Upper bound of the lightest neutral Higgs mass in extended supersymmetric Standard Models. *Phys. Lett. B* **295**, 73–78 (1992). [https://doi.org/10.1016/0370-2693\(92\)90091-H](https://doi.org/10.1016/0370-2693(92)90091-H)
- S.P. Martin, Extra vector-like matter and the lightest Higgs scalar boson mass in low-energy supersymmetry. *Phys. Rev. D* **81**, 035004 (2010). <https://doi.org/10.1103/PhysRevD.81.035004> arXiv:0910.2732
- K.S. Babu, I. Gogoladze, M.U. Rehman, Q. Shafi, Higgs Boson mass, Sparticle spectrum and little hierarchy problem in extended MSSM. *Phys. Rev. D* **78**, 055017 (2008). <https://doi.org/10.1103/PhysRevD.78.055017> arXiv:0807.3055
- S.P. Martin, Raising the Higgs Mass with Yukawa couplings for isotriplets in vector-like extensions of minimal supersymmetry. *Phys. Rev. D* **82**, 055019 (2010). <https://doi.org/10.1103/PhysRevD.82.055019> arXiv:1006.4186
- P.W. Graham, A. Ismail, S. Rajendran, P. Saraswat, A little solution to the little hierarchy problem: a vector-like generation. *Phys. Rev. D* **81**, 055016 (2010). <https://doi.org/10.1103/PhysRevD.81.055016> arXiv:0910.3020
- J. Kang, P. Langacker, B.D. Nelson, Theory and phenomenology of exotic isosinglet quarks and squarks. *Phys. Rev. D* **77**, 035003 (2008). <https://doi.org/10.1103/PhysRevD.77.035003> arXiv:0708.2701
- L. Randall, R. Sundrum, A Large mass hierarchy from a small extra dimension. *Phys. Rev. Lett.* **83**, 3370–3373 (1999). <https://doi.org/10.1103/PhysRevLett.83.3370> arXiv:hep-ph/9905221
- L. Randall, R. Sundrum, An alternative to compactification. *Phys. Rev. Lett.* **83**, 4690–4693 (1999). <https://doi.org/10.1103/PhysRevLett.83.4690> arXiv:hep-th/9906064
- K. Agashe, G. Perez, A. Soni, Flavor structure of warped extra dimension models. *Phys. Rev. D* **71**, 016002 (2005). <https://doi.org/10.1103/PhysRevD.71.016002> arXiv:hep-ph/0408134
- K. Agashe, G. Perez, A. Soni, Collider signals of top quark flavor violation from a warped extra dimension. *Phys. Rev. D* **75**, 015002 (2007). <https://doi.org/10.1103/PhysRevD.75.015002> arXiv:hep-ph/0606293
- T. Li, Z. Murdock, S. Nandi, S.K. Rai, Quark lepton unification in higher dimensions. *Phys. Rev. D* **85**, 076010 (2012). <https://doi.org/10.1103/PhysRevD.85.076010> arXiv:1201.5616
- G.-Y. Huang, K. Kong, S.C. Park, Bounds on the Fermion-bulk masses in models with universal extra dimensions. *JHEP* **06**, 099 (2012). [https://doi.org/10.1007/JHEP06\(2012\)099](https://doi.org/10.1007/JHEP06(2012)099) arXiv:1204.0522
- C. Biggio, F. Feruglio, I. Masina, M. Perez-Victoria, Fermion generations, masses and mixing angles from extra dimensions. *Nucl. Phys. B* **677**, 451–470 (2004). <https://doi.org/10.1016/j.nuclphysb.2003.10.052> arXiv:hep-ph/0305129

21. D.E. Kaplan, T.M.P. Tait, Supersymmetry breaking, fermion masses and a small extra dimension. *JHEP* **06**, 020 (2000). <https://doi.org/10.1088/1126-6708/2000/06/020> arXiv:hep-ph/0004200
22. H.-C. Cheng, Doublet triplet splitting and fermion masses with extra dimensions. *Phys. Rev. D* **60**, 075015 (1999). <https://doi.org/10.1103/PhysRevD.60.075015> arXiv:hep-ph/9904252
23. R.S. Chivukula, B.A. Dobrescu, H. Georgi, C.T. Hill, Top quark seesaw theory of electroweak symmetry breaking. *Phys. Rev. D* **59**, 075003 (1999). <https://doi.org/10.1103/PhysRevD.59.075003> arXiv:hep-ph/9809470
24. B.A. Dobrescu, C.T. Hill, Electroweak symmetry breaking via top condensation seesaw. *Phys. Rev. Lett.* **81**, 2634–2637 (1998). <https://doi.org/10.1103/PhysRevLett.81.2634> arXiv:hep-ph/9712319
25. H.-J. He, C.T. Hill, T.M.P. Tait, Top quark seesaw, vacuum structure and electroweak precision constraints. *Phys. Rev. D* **65**, 055006 (2002). <https://doi.org/10.1103/PhysRevD.65.055006> arXiv:hep-ph/0108041
26. R. Contino, L. Da Rold, A. Pomarol, Light custodians in natural composite Higgs models. *Phys. Rev. D* **75**, 055014 (2007). <https://doi.org/10.1103/PhysRevD.75.055014> arXiv:hep-ph/0612048
27. C. Anastasiou, E. Furlan, J. Santiago, Realistic composite Higgs models. *Phys. Rev. D* **79**, 075003 (2009). <https://doi.org/10.1103/PhysRevD.79.075003> arXiv:0901.2117
28. K. Kong, M. McCaskey, G.W. Wilson, Multi-lepton signals from the top-prime quark at the LHC. *JHEP* **04**, 079 (2012). [https://doi.org/10.1007/JHEP04\(2012\)079](https://doi.org/10.1007/JHEP04(2012)079) arXiv:1112.3041
29. M. Gillioz, R. Grober, C. Grojean, M. Muhlleitner, E. Salvioni, Higgs low-energy theorem (and its corrections) in composite models. *JHEP* **10**, 004 (2012). [https://doi.org/10.1007/JHEP10\(2012\)004](https://doi.org/10.1007/JHEP10(2012)004) arXiv:1206.7120
30. N. Arkani-Hamed, A.G. Cohen, E. Katz, A.E. Nelson, The littlest Higgs. *JHEP* **07**, 034 (2002). arXiv:hep-ph/0206021
31. M. Perelstein, M.E. Peskin, A. Pierce, Top quarks and electroweak symmetry breaking in little Higgs models. *Phys. Rev. D* **69**, 075002 (2004). <https://doi.org/10.1103/PhysRevD.69.075002> arXiv:hep-ph/0310039
32. M. Carena, J. Hubisz, M. Perelstein, P. Verdier, Collider signature of T-quarks. *Phys. Rev. D* **75**, 091701 (2007). <https://doi.org/10.1103/PhysRevD.75.091701> arXiv:hep-ph/0610156
33. S. Matsumoto, T. Moroi, K. Tobe, Testing the littlest Higgs model with T-parity at the large hadron collider. *Phys. Rev. D* **78**, 055018 (2008). <https://doi.org/10.1103/PhysRevD.78.055018> arXiv:0806.3837
34. T. Han, H.E. Logan, B. McElrath, L.-T. Wang, Phenomenology of the little Higgs model. *Phys. Rev. D* **67**, 095004 (2003). <https://doi.org/10.1103/PhysRevD.67.095004> arXiv:hep-ph/0301040
35. S. Bahrami, M. Frank, Dark matter in the Higgs triplet model. *Phys. Rev. D* **91**, 075003 (2015). <https://doi.org/10.1103/PhysRevD.91.075003> arXiv:1502.02680
36. N.F. Bell, M.J. Dolan, L.S. Friedrich, M.J. Ramsey-Musolf, R.R. Volkas, Electroweak Baryogenesis with vector-like leptons and scalar singlets. *JHEP* **19**, 012 (2020). [https://doi.org/10.1007/JHEP09\(2019\)012](https://doi.org/10.1007/JHEP09(2019)012) arXiv:1903.11255
37. E. Osoba, Fourth Generations with an Inert Doublet Higgs. arXiv:1206.6912
38. S.K. Garg, C.S. Kim, Vector like leptons with extended Higgs sector. arXiv:1305.4712
39. A. Angelescu, G. Arcadi, Dark matter phenomenology of SM and enlarged higgs sectors extended with vector like leptons. *Eur. Phys. J. C* **77**, 456 (2017). <https://doi.org/10.1140/epjc/s10052-017-5015-2> arXiv:1611.06186
40. A. Angelescu, A. Djouadi, G. Moreau, Scenarii for interpretations of the LHC diphoton excess: two Higgs doublets and vector-like quarks and leptons. *Phys. Lett. B* **756**, 126–132 (2016). <https://doi.org/10.1016/j.physletb.2016.02.064> arXiv:1512.04921
41. S. Bahrami, M. Frank, Vector leptons in the Higgs triplet model. *Phys. Rev. D* **88**, 095002 (2013). <https://doi.org/10.1103/PhysRevD.88.095002> arXiv:1308.2847
42. S. Bahrami, M. Frank, Neutrino dark matter in the Higgs triplet model, in *Meeting of the APS Division of Particles and Fields*, 9 (2015). arXiv:1509.04763
43. S. Chakdar, K. Ghosh, S. Nandi, S.K. Rai, Collider signatures of mirror fermions in the framework of a left-right mirror model. *Phys. Rev. D* **88**, 095005 (2013). <https://doi.org/10.1103/PhysRevD.88.095005> arXiv:1305.2641
44. S. Bahrami, M. Frank, D.K. Ghosh, N. Ghosh, I. Saha, Dark matter and collider studies in the left-right symmetric model with vector-like leptons. *Phys. Rev. D* **95**, 095024 (2017). <https://doi.org/10.1103/PhysRevD.95.095024> arXiv:1612.06334
45. A. Patra, S.K. Rai, Lepton-specific universal seesaw model with left-right symmetry. *Phys. Rev. D* **98**, 015033 (2018). <https://doi.org/10.1103/PhysRevD.98.015033> arXiv:1711.00627
46. D. Das, U.K. Dey, P.B. Pal, Quark mixing in an S_3 symmetric model with two Higgs doublets. *Phys. Rev. D* **96**, 031701 (2017). <https://doi.org/10.1103/PhysRevD.96.031701> arXiv:1705.07784
47. D. Cogollo, J.A.P. Silva, Two Higgs doublet models with an S_3 symmetry. *Phys. Rev. D* **93**, 095024 (2016). <https://doi.org/10.1103/PhysRevD.93.095024> arXiv:1601.02659
48. I. Chakraborty, D.K. Ghosh, N. Ghosh, S.K. Rai, Dark matter and collider searches in S_3 -symmetric 2HDM with vector like lepton. *Eur. Phys. J. C* **81**, 679 (2021). <https://doi.org/10.1140/epjc/s10052-021-09446-5> arXiv:2104.03351
49. *The International Linear Collider Technical Design Report-Volume 1: Executive Summary*. arXiv:1306.6327
50. *The International Linear Collider Technical Design Report-Volume 2: Physics*. arXiv:1306.6352
51. ATLAS collaboration, G. Aad et al., Search for electroweak production of charginos and sleptons decaying into final states with two leptons and missing transverse momentum in $\sqrt{s} = 13$ TeV pp collisions using the ATLAS detector. *Eur. Phys. J. C* **80**, 123 (2020). <https://doi.org/10.1140/epjc/s10052-019-7594-6> arXiv:1908.08215
52. ATLAS collaboration, M. Aaboud et al., Search for supersymmetry in events with four or more leptons in $\sqrt{s} = 13$ TeV pp collisions with ATLAS. *Phys. Rev. D* **98**, 032009 (2018). <https://doi.org/10.1103/PhysRevD.98.032009> arXiv:1804.03602
53. ATLAS collaboration, G. Aad et al., Search for doubly and singly charged Higgs bosons decaying into vector bosons in multi-lepton final states with the ATLAS detector using proton–proton collisions at $\sqrt{s} = 13$ TeV. arXiv:2101.11961
54. ATLAS Collaboration collaboration, Search for squarks and gluinos in final states with jets and missing transverse momentum using 139 fb⁻¹ of $\sqrt{s} = 13$ TeV pp collision data with the ATLAS detector, tech. rep., CERN, Geneva, Aug (2019)
55. A. Alloul, N.D. Christensen, C. Degrande, C. Duhr, B. Fuks, FeynRules 2.0: A complete toolbox for tree-level phenomenology. *Comput. Phys. Commun.* **185**, 2250–2300 (2014). <https://doi.org/10.1016/j.cpc.2014.04.012> arXiv:1310.1921
56. A. Belyaev, N.D. Christensen, A. Pukhov, CalcHEP 3.4 for collider physics within and beyond the Standard Model. *Comput. Phys. Commun.* **184**, 1729–1769 (2013). <https://doi.org/10.1016/j.cpc.2013.01.014> arXiv:1207.6082
57. G. Bélanger, F. Boudjema, A. Pukhov, A. Semenov, micrOMEGAs4.1: two dark matter candidates. *Comput. Phys. Commun.* **192**, 322–329 (2015). <https://doi.org/10.1016/j.cpc.2015.03.003> arXiv:1407.6129
58. Planck collaboration, N. Aghanim et al., Planck 2018 results. VI. Cosmological parameters. *Astron. Astrophys.* **641**, A6 (2020). <https://doi.org/10.1051/0004-6361/201833910> arXiv:1807.06209

59. LUX collaboration, D.S. Akerib et al., Results from a search for dark matter in the complete LUX exposure. *Phys. Rev. Lett.* **118**, 021303 (2017). <https://doi.org/10.1103/PhysRevLett.118.021303>. arXiv:1608.07648
60. PICO collaboration, C. Amole et al., Dark Matter Search Results from the Complete Exposure of the PICO-60 C₃F₈ Bubble Chamber. *Phys. Rev. D* **100**, 022001 (2019). <https://doi.org/10.1103/PhysRevD.100.022001>. arXiv:1902.04031
61. T. Daylan, D.P. Finkbeiner, D. Hooper, T. Linden, S.K.N. Portillo, N.L. Rodd et al., The characterization of the gamma-ray signal from the central Milky Way: a case for annihilating dark matter. *Phys. Dark Univ.* **12**, 1–23 (2016). <https://doi.org/10.1016/j.dark.2015.12.005> arXiv:1402.6703
62. MAGIC, Fermi-LAT collaboration, M.L. Ahnen et al., Limits to Dark Matter Annihilation Cross-Section from a Combined Analysis of MAGIC and Fermi-LAT Observations of Dwarf Satellite Galaxies. *JCAP* **02**, 039 (2016). <https://doi.org/10.1088/1475-7516/2016/02/039>. arXiv:1601.06590
63. J. Alwall, R. Frederix, S. Frixione, V. Hirschi, F. Maltoni, O. Mattelaer et al., The automated computation of tree-level and next-to-leading order differential cross sections, and their matching to parton shower simulations. *JHEP* **07**, 079 (2014). [https://doi.org/10.1007/JHEP07\(2014\)079](https://doi.org/10.1007/JHEP07(2014)079) arXiv:1405.0301
64. DELPHES 3 collaboration, J. de Favereau, C. Delaere, P. Demin, A. Giammanco, V. Lemaître, A. Mertens et al., DELPHES 3, A modular framework for fast simulation of a generic collider experiment. *JHEP* **02**, 057 (2014). [https://doi.org/10.1007/JHEP02\(2014\)057](https://doi.org/10.1007/JHEP02(2014)057). arXiv:1307.6346
65. DELPHES 3 collaboration, J. de Favereau, C. Delaere, P. Demin, A. Giammanco, V. Lemaître, A. Mertens et al., DELPHES 3, A modular framework for fast simulation of a generic collider experiment. *JHEP* **02**, 057 (2014). [https://doi.org/10.1007/JHEP02\(2014\)057](https://doi.org/10.1007/JHEP02(2014)057). arXiv:1307.6346
66. A. Hocker et al., TMVA-toolkit for multivariate data analysis. arXiv:physics/0703039
67. J. Beyer, J. List, Interplay of beam polarisation and systematic uncertainties at future e^+e^- colliders, in *European Physical Society Conference on High Energy Physics 2021*, 11 (2021). arXiv:2111.06687
68. A. Adhikary, N. Chakrabarty, I. Chakraborty, J. Lahiri, Probing the $H^\pm W^\mp Z$ interaction at the high energy upgrade of the LHC. *Eur. Phys. J. C* **81**, 554 (2021). <https://doi.org/10.1140/epjcs/10052-021-09335-x> arXiv:2010.14547